Comparative angle-resolved photoemission spectroscopy study of $CaRuO_3$ and $SrRuO_3$ thin films: Pronounced spectral weight transfer and possible precursor of lower Hubbard band

H. F. Yang,[1,2] C. C. Fan,[1,2] Z. T. Liu,[1,2] Q. Yao,[1,3] M. Y. Li,[1,2] J. S. Liu,[1,2] M. H. Jiang,[1] and D. W. Shen[1,2,*]

[1]*State Key Laboratory of Functional Materials for Informatics, Shanghai Institute of Microsystem and Information Technology (SIMIT), Chinese Academy of Sciences, Shanghai 200050, China*

[2]*CAS-Shanghai Science Research Center, Shanghai 201203, China*

[3]*State Key Laboratory of Surface Physics, Department of Physics, and Advanced Materials Laboratory, Fudan University, Shanghai 200433, China*

(Received 20 May 2016; revised manuscript received 29 July 2016; published 23 September 2016)

In the prototypical 4*d* system (Sr,Ca)RuO_3, the degree and origin of electron correlations, and how they correlate with physical properties, still remain elusive, though extensive studies have been performed. In this work we present a comparative electronic structure study of high-quality epitaxial $CaRuO_3$ and $SrRuO_3$ thin films, by means of reactive molecular beam epitaxy and *in situ* angle-resolved photoemission spectroscopy. We found that while $SrRuO_3$ possesses sharp features signaling the Fermi liquid state, the isostructural $CaRuO_3$ exhibits broad features and its spectral weight is markedly transferred from the Fermi level to −1.2 eV forming a "hump" structure which resembles the Mott-Hubbard system (Sr,Ca)VO_3. We suggest that this hump is the precursor of the lower Hubbard band, and the U/W (U and W represent the on-site Coulomb interactions and bandwidth, respectively) of our $CaRuO_3$ thin film is much larger than that of $SrRuO_3$. In addition, we discuss the origin of electron correlations as well as the ferromagnetism in $SrRuO_3$ which is absent in $CaRuO_3$. Our findings put constraints on future studies, and also show that perovskite ruthenates are indeed an experimentally tunable system for the study of electron correlations.

DOI: 10.1103/PhysRevB.94.115151

I. INTRODUCTION

The physics of electron correlations is one of the most fundamental topics in the study of transition metal oxides, since it essentially lays the foundation for versatile extraordinary physical phenomena including high-T_c superconductivity [1,2], metal-insulator transitions [3], and colossal magnetoresistance [4], etc.

The celebrated single-band Hubbard model addresses the role of on-site Coulomb interaction U of electrons. The Mott-Hubbard transition illustrates that when the U is large enough to be comparable with the bandwidth W, the half-filled band will be split into the upper and lower Hubbard bands separated by a considerable band gap, and the system will be driven into the Mott insulating state [3,5]. Such a well-known example is the $3d^1$ electron system (Sr,Ca)VO_3. Although this system would not reach the real insulating state through continuous Ca substitution, the pronounced spectral weight transfer from the Fermi level (E_F) towards high binding energy region and the resulted lower Hubbard band located at around −1.6 eV have been directly observed by photoemission studies [6–8]. When going from 3*d* to 4*d* electron systems, U would usually decrease since 4*d* electrons are expected to be more delocalized than 3*d* ones, while the spin-orbit coupling (SOC) would become stronger due to the heavier elements.

Among various 4*d* transition metal oxides, perovskite ruthenium (Ru) oxides $CaRuO_3$ (CRO) and $SrRuO_3$ (SRO) have aroused plenty of interest, since they not only serve as key building bricks in all-oxide electronics and spintronics but also can provide rich implications for fundamental physics [9]. In these compounds, Ru^{4+} has a $4d^4$ configuration with four electrons occupying three degenerate t_{2g} orbitals. Despite their similar crystal structure, while SRO is a metallic ferromagnet with a T_c of 160 K and exhibits the Fermi-liquid (FL) state at low temperatures [9,10], CRO remains metallic with the absence of long-range magnetic orderings and does not exhibit FL behaviors until 1.5 K [11–13]. So far, electron correlations have been proposed to account for such striking differences [9,14,15]. However, controversies on the extent of electron correlations and how they determine the physical properties still exist, despite a magnitude of theoretical [15–21] and experimental attempts [10,22–31]. Additionally, the origin of electron correlations in this system remains an open question. Besides the common Coulomb repulsion (Mott physics), the Hund's coupling [16,32,33] and SOC [34] were also proposed to play an important role.

In order to study electron correlations in CRO and SRO, directly detecting their electronic structures is highly desirable. However, the difficulty to cleave the pseudocubic (Sr,Ca)RuO_3 highly hinders the visualization of their band structures by means of experimental probes like scanning tunneling spectroscopy (STS) and angle-resolved photoemission spectroscopy (ARPES). To the best of our knowledge, the measured band structure of CRO has not been reported before. And thus, a comparable picture of low-lying electronic structures of CRO and SRO is still lacking to date.

In this article we took advantage of reactive molecular beam epitaxy (MBE) and *in situ* ARPES [10,35,36] to investigate the band structures of CRO and SRO in a comparative way. We found that, while SRO exhibits sharp spectra formed by evident quasiparticles near E_F signaling the FL state, the photoemission spectra of CRO show broad and blurry features in the vicinity of E_F and a pronounced "hump" structure centered at −1.2 eV which we suggest is the precursor of the lower Hubbard band.

*dwshen@mail.sim.ac.cn

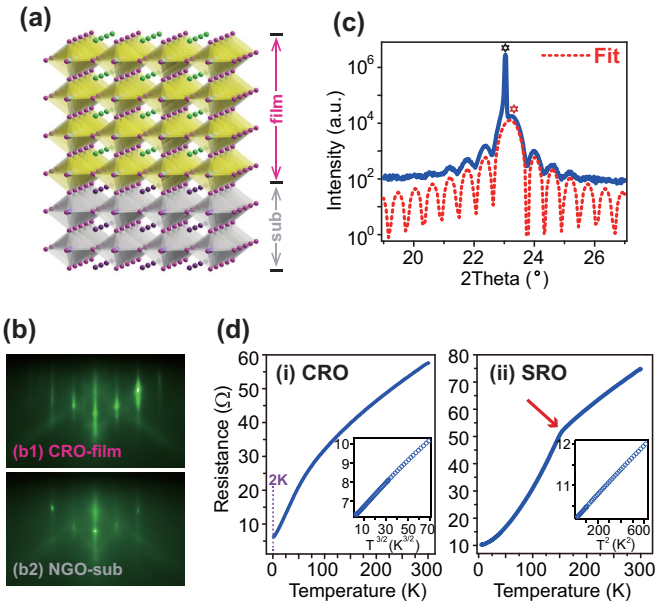

FIG. 1. Growth and characterization of CRO thin films. (a) Schematic of CRO thin films epitaxially grown on NGO substrates. (b) Typical RHEED patterns of CRO thin film (b1) and the NGO substrate (b2) along the $(100)_p$ azimuthal. Sharp diffraction spot-streak structures and visible Kikuchi lines in the CRO RHEED pattern indicate its high quality with long-range ordered surface structure. (c) X-ray diffraction pattern around $(001)_p$ peak for a CRO thin film. The red and black markers denote $(001)_p$ peaks of the CRO thin film and the NGO substrate, respectively. The red dotted line is the good fitting curve which gives a thickness of 41 unit cells (UCs) and out-of-plane constant of 3.832 Å as a result of the tensile strain. (d) Temperature dependence of the resistances of this 41-UC-thick CRO film (i) and 21-UC-thick SRO film (ii). In (i), no signature of a phase transition in our CRO film was observed within the temperature range of our measurement; the inset shows that the low-temperature resistance has a linear dependence of $T^{3/2}$ (T is short for temperature). In (ii), the red arrow marks the kink corresponding to the ferromagnetic transition of SRO; the inset shows that the low-temperature resistance has a linear dependence of T^2, which indicates the Fermi liquid ground state. The growth details of high-quality SRO thin films with well-controlled thicknesses can be found in our previous work [34].

II. EXPERIMENT

Perovskite $(001)_p$ (where the subscript p denotes pseudocubic indices) CRO films [Fig. 1(a)] were fabricated using a DCA R450 OMBE system at a substrate temperature of 750 °C in a background pressure of 2×10^{-6} Torr of distilled ozone. Ca and Ru were evaporated from an effusion cell and an electron beam evaporator, respectively. To achieve high-quality CRO thin films, $(001)_p$ $NdGaO_3$ (NGO) was used as the substrate to effectively get rid of multidomains [37], which leads to a 0.6% tensile strain for epitaxial films. During growth, *in situ* surface-sensitive reflection high-energy electron diffraction (RHEED) was used to monitor the growth and check surface structure. Growth details of our high-quality SRO thin films can be found in our previous work [35].

After growth, thin films were quickly transferred to the combined ARPES chamber (within 5 min) for measurements through an ultrahigh vacuum buffer chamber ($\sim1.0\times10^{-10}$ Torr). Our in-house ARPES system is equipped with a VG-Scienta R8000 electron analyzer and a SPECS UVLS helium discharging lamp with a monochromator. The data were collected at 15 K with He Iα (21.2 eV) photons under ultrahigh vacuum of 8×10^{-11} Torr. The overall energy and angular resolutions were set to 15 meV and 0.3°, respectively. During the measurements, the films were checked to be stable and no signatures of degradation or charging were observed.

III. RESULTS AND DISCUSSIONS

As displayed in Fig. 1(b1), the RHEED pattern of a typical CRO thin film features shiny diffraction spot-streak structures and visible Kikuchi lines which are comparable to the NGO single-crystalline substrate [Fig. 1(b2)]. These fine structures of RHEED pattern reveal the high quality of films with long-range ordered lattice structure and flat surface, which guarantee the following good ARPES data. Figure 1(c) shows the typical x-ray diffraction (XRD) θ-2θ scan of the CRO film around the $(001)_p$ peak. One can see persistent fringes which indicate the sharp and smooth interface between the thin film and the substrate that again confirms the high quality of thin films. Good fitting to these fringes [see the red dotted line in Fig. 1(c)] gives a thickness of 41 unit cells (UCs) and the out-of-plane constant of 3.832 Å as a result of the tensile strain from the NGO substrate. Characterizations of SRO films have been reported in our previous work [35].

Figure 1(d)(i) displays the temperature dependence of the electrical resistance $[R(T)]$ of this 41-UC-thick CRO film. CRO remains metallic in the whole temperature range (from 2.0 to 300 K), and exhibits a smooth curve without the kinklike feature, suggesting no signature of long-range magnetic ordering as in SRO [9,10]. Moreover, in our measurement range, the low-temperature resistivity obeys a $T^{3/2}$ dependence, implying the non-Fermi-liquid (NFL) state. This behavior as well as the $R(T)$ curve shape, is in accordance with previous reports [11–13]. By contrast, SRO is generally thought to possess the FL ground state [i.e., low-temperature resistance obeys a T^2 dependence; see the inset of Fig. 1(d)(ii)] with a ferromagnetic transition around 155 K signaled by a "kink" (marked by the red arrow) in the $R(T)$ curve [9,10].

To understand these differences between the isostructural CRO and SRO thin films, *in situ* ARPES measurements were carried out to compare their low-lying electronic structures. Figures 2(a) and 2(b) show the representative valence band (VB) spectra of CRO and SRO along the (0, 0)-(0, π) high symmetry direction [see the cut #1 in the inset of Fig. 2(b)] and the corresponding integrated energy dispersive curves (EDCs) [normalization within (−4.2 eV, −3.4 eV) was used to display the near-E_F features clearly], respectively. Evident dispersive bands can be observed, which again confirms the high-quality surface and crystal structures of the thin film. High-energy parts of their band dispersions (from −2.5 to −7.5 eV) look quite similar, as illustrated by their spectra in Fig. 2(a). However, near E_F [cyan shadow region in Fig. 2(b)], a pronounced difference is directly revealed from the integrated EDCs, whereas SRO shows one sharp peak at E_F, CRO exhibits one peak at E_F and an additional

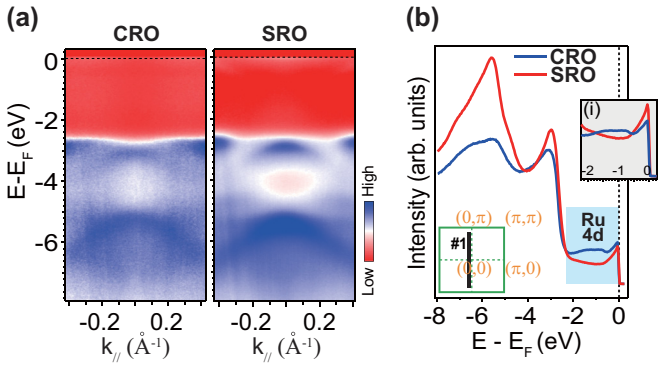

FIG. 2. Valence bands of CRO and SRO. (a) Valence band spectra of CRO and SRO. Their high-binding energy dispersions (below −2.4 eV) are similar. (b) Integrated valence bands of CRO (blue curve) and SRO (red curve). The normalization of these two curves was done within the energy window of [−4.2 eV, −3.4 eV] to clearly show their near-E_F structures. In (i), near-E_F parts were shown with the normalization within the energy window of [−2.2 eV, 0]. The inset is the schematic of the first Brillouin zone (corresponding to the pseudocubic substrate) with the cut #1.

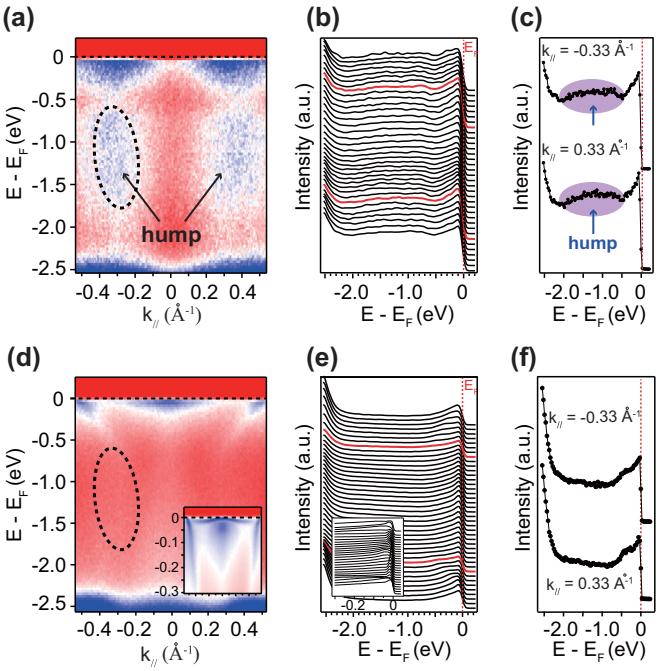

FIG. 3. Side-by-side comparison of representative long-cut dispersions of CRO and SRO along the cut #1. (a) Long-cut spectrum (down to −2.5 eV) of CRO. The hump structure enclosed by black dotted line is evidently shown to be located around −1.2 eV. (b) EDCs of the spectrum (a) exhibiting broad peaks. (c) Two representative EDCs cutting across the hump structure marked by the purple shadow. (d) Long-cut spectrum of SRO. No hump structure is observed [no evident spectral weight in the same black-dotted-line region as (a)]. The inset shows sharp band dispersions near E_F. (e) EDCs of the spectrum (d), exhibiting sharp peaks. The inset shows EDCs near E_F. (f) Two representative EDCs at the same positions as (c) showing no signatures of hump in SRO.

hump structure centered at −1.2 eV. These differences are also shown in the zoom-in plot [Fig. 2(b)(i)], in which the normalization within (−2.2 eV, 0) was used. Note that bands in this region mainly originate from Ru 4*d* electrons. It is worth noting that spectra backgrounds of CRO and SRO can be intrinsically different, and generally a high-binding-energy region has a higher background than the near-E_F region within one spectrum.

Then we investigated the band dispersions of CRO and SRO in the vicinity of E_F, as directly compared in Fig. 3. While SRO shows sharp band dispersions built by evident quasiparticles around E_F [10,35] [insets of Figs. 3(d) and 3(e)], CRO displays blurry and broad features which reveals that electrons (quasiparticles) have quite short lifetimes [Figs. 3(a) and 3(b)]. This finding indicates the NFL state of CRO and FL state of SRO at our measurement temperature (15 K), which is in line with bulk-sensitive transport studies discussed above. Moreover, in contrast to SRO, CRO possesses appreciable spectral weight around −1.2 eV forming an ellipsoid-shaped band [Fig. 3(a)]. This additional feature contributes to the pronounced hump structure, which is as also confirmed by the side-by-side comparison of individual EDCs [Figs. 3(c) and 3(f)].

What's the origin of the hump feature discovered in CRO thin film? Since this hump resides at relatively high binding energy region (more than 1.0 eV below E_F), low-energy excitations which may exist in this system (e.g., phonons [35], polarons [38], and magnons [2]) should not be attributed to. If we compare the renormalized integrated EDCs of CRO and SRO [Fig. 4(a)], we can conjecture that part of spectral weight of the quasiparticle peak near E_F should have shifted to −1.2 eV and formed the hump structure in CRO. This is naturally reminiscent of the well-established example—Sr(Ca)VO_3 system with a simple $3d^1$ configuration [3]. As displayed in Fig. 4(b)(i), $SrVO_3$ shows a coherent peak at E_F and a broad feature centered at −1.6 eV ascribed to the lower Hubbard band; when going from $SrVO_3$ to $CaVO_3$, the effective Coulomb interaction increases and consequently more spectral weight transfers from the coherent peak to the lower Hubbard band at higher binding energy [6–8]. Such behavior was also observed in some other typical Mott-Hubbard systems, such as V_2O_3 [39] and $NiS_{2-x}Se_x$ [40]. Theoretically, Mott-Hubbard spectral weight transferring has been studied in the context of the dynamical mean field theory (DMFT) solution of the Hubbard model [41,42]. As schematically shown in Fig. 4(b)(ii), as increasing Coulomb interactions between electrons, spectral features evolve from sharp peak at E_F [electrons are entirely independent which is characteristic of a "good" metal (see the curve *a*)] to the vanishing of the quasiparticle peak and the formation of incoherent lower Hubbard band [electrons hugely interact with each other which is characteristic of Mott insulator (see the curve *f*)]; in the mediate region, the spectrum features a quasiparticle peak near E_F and a broad hump which is the precursor of the lower Hubbard band.

Likewise, the spectral weight transferring of CRO could be understood in the similar Mott physics picture, and the hump of CRO can be ascribed to the lower Hubbard band. Actually, its cousin compound Ca_2RuO_4 is a well-studied Mott insulator [43,44], and doping SRO showed similar spectral weight transfer which was interpreted to be related

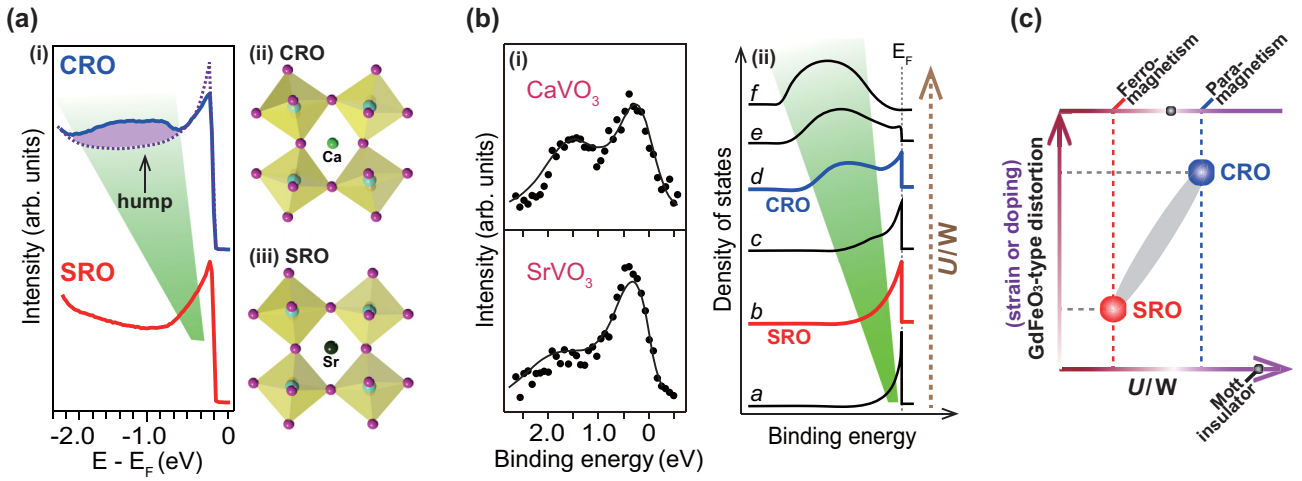

FIG. 4. (a) Integrated EDCs of CRO (blue curve) and SRO (red curve) (i), and schematic of CRO (ii) showing a bigger $GdFeO_3$-type distortion than SRO (iii). (b) Pronounced spectral weight transfer in Mott-Hubbard system Sr(Ca)VO_3, which is reproduced from Ref. [7] (i). Schematic of spectral weight transfer with increasing the U/W in a typical Mott-Hubbard system (from the DMFT solution of the Hubbard model; Refs. [41,42]) (ii). (c) Simple phase diagram of CRO and SRO. The y axis and the bottom and top x axes are the $GdFeO_3$-type distortion and the U/W and magnetism, respectively. Ruthenium perovskites are indeed a tunable system to explore the electron correlations and related quantum criticality, with structural distortion as the knob (can be experimentally modified via epitaxial strain and doping).

with correlation effects [24,25]. Therefore, it is reasonable to demonstrate that the Mott physics plays an important role in the formation of the hump in CRO, and CRO shows a larger U/W than SRO [see Fig. 4(b)(ii)]. From the perspective of structural distortion, smaller size of Ca^{2+} than Sr^{2+} leads to bigger $GdFeO_3$-type distortion in CRO [Fig. 4(a)], and further suppresses the hopping of electrons (decreases the bandwidth W), and thus increases the effective Coulomb interactions [14,15,31,33].

Since C(S)RO are 4d non-half-filled multiband compounds, besides Mott physics, some other scenarios were proposed to play a role in electron correlations. On one hand, recently initiated by the studies of iron-based superconductors [45,46], Hund's rule coupling (intra-atomic exchange J) was proposed to play a key role in determining the electron correlations from two aspects: it drives the system away from the Mott transition and decreases the possible Mott gap; meanwhile, it makes the metallic state more correlated by strongly suppressing the quasiparticle coherence scale [16,32]. Considering the multiband nature and highly suppressed coherence temperature of CRO, it may also contribute to the electron correlations [16,33]. On the other hand, SOC was also involved into the strongly correlated physics (e.g., spin-orbit Mott insulator): the split bands by SOC are so narrow that a small on-site Coulomb interaction U may introduce a relatively large U/W which drives the system into the Mott insulating state [34]. Since Ru possesses a stronger SOC than 3d elements, it is reasonable to take SOC into consideration. However, our photoemission data do not reveal any notable splitting phenomena of bands near E_F of C(S)RO, which is consistent with previous theoretical predictions that SOC would not have a large effect on the electronic structure [14,18].

Except the hump structure, another pronounced difference in the band structures of CRO and SRO is the flat band around the BZ center of SRO which is absent in CRO. These bands contribute to large density of states, which together with the FL ground state, may account for the itinerant ferromagnetism of SRO [17,47]. Note that local moment may also play a role [10,21], regarding the Hund's coupling in the non-half-filled shells. Although CRO does not show any long-range magnetic ordering (in our thin film case and bulk studies reported [11,12]), it was suggested to be located in the vicinity of magnetic ordering region [12,17]. Recently, ferromagnetic CRO thin film was reported by applying considerable tensile strain [48] possibly due to modifying structural distortion. Meanwhile, strain was also suggested to change the Curie temperature of SRO [49].

Figure 4(d) displays a simple phase diagram of ruthenium perovskites. The y axis and top and bottom x axes represent the $GdFeO_3$-type distortion and magnetism and the U/W, respectively. With the increase of the $GdFeO_3$-type distortion, the system can evolve from a ferromagnet (bulk SRO) with FL ground state and small effective Coulomb interaction, to a nonmagnet (bulk CRO) with NFL ground state and big effective Coulomb interaction. Thus, a quantum critical point is expected in the mediate region, and the $GdFeO_3$-type distortion can be used as an essential knob. This distortion can be experimentally tuned via epitaxial strain [10,48,49] and chemical doping [24,25,50–52]. Therefore, ruthenium perovskites are indeed a profound system to study the electron correlations and relevant quantum criticality.

IV. CONCLUSION

To summarize, comparative *in situ* ARPES studies of high-quality CRO and SRO thin films were presented. In contrast to SRO possessing sharp features at the Fermi level, CRO exhibits broad features and the spectral weight is substantially transferred from E_F to around -1.2 eV forming a hump

structure which we suggest is the precursor of lower Hubbard band. We show that the U/W of CRO thin films on NGO is bigger than that of SRO. Discussions about the possible origins of the electron correlations and magnetism are also presented. Our results suggest that ruthenium perovskites are indeed a tunable system to study the electron correlations and quantum criticality therein. Further studies from both theoretical and experimental aspects are highly advocated, and our results could be a good start point.

ACKNOWLEDGMENTS

We gratefully acknowledge the discussions with Professor D. J. Singh. This work is supported by the National Key R&D Program of the MOST of China (Grant No. 2016YFA0300204) and the National Science Foundation of China (Grants No. 11274332, No. 11574337, and No. 11227902). D.W.S. is also supported by the "Strategic Priority Research Program (B)" of the Chinese Academy of Sciences (Grant No. XDB04040300) and the "Youth Innovation Promotion Association CAS."

[1] P. A. Lee, N. Nagaosa, and X.-G. Wen, Rev. Mod. Phys. **78**, 17 (2006).
[2] A. Damascelli, Z. Hussain, and Z.-X. Shen, Rev. Mod. Phys. **75**, 473 (2003).
[3] M. Imada, A. Fujimori, and Y. Tokura, Rev. Mod. Phys. **70**, 1039 (1998).
[4] M. B. Salamon and M. Jaime, Rev. Mod. Phys. **73**, 583 (2001).
[5] P. W. Anderson, Phys. Rev. **115**, 2 (1959).
[6] I. H. Inoue, I. Hase, Y. Aiura, A. Fujimori, Y. Haruyama, T. Maruyama, and Y. Nishihara, Phys. Rev. Lett. **74**, 2539 (1995).
[7] K. Maiti, D. D. Sarma, M. J. Rozenberg, I. H. Inoue, H. Makino, O. Goto, M. Pedio, and R. Cimino, Europhys. Lett. **55**, 246 (2001).
[8] K. Maiti, U. Manju, S. Ray, P. Mahadevan, I. H. Inoue, C. Carbone, and D. D. Sarma, Phys. Rev. B **73**, 052508 (2006).
[9] G. Koster, L. Klein, W. Siemons, G. Rijnders, J. S. Dodge, C. B. Eom, D. H. A. Blank, and M. R. Beasley, Rev. Mod. Phys. **84**, 253 (2012).
[10] D. E. Shai, C. Adamo, D. W. Shen, C. M. Brooks, J. W. Harter, E. J. Monkman, B. Burganov, D. G. Schlom, and K. M. Shen, Phys. Rev. Lett. **110**, 087004 (2013).
[11] L. Klein, L. Antognazza, T. H. Geballe, M. R. Beasley, and A. Kapitulnik, Phys. Rev. B **60**, 1448 (1999).
[12] G. Cao, O. Korneta, S. Chikara, L. E. Delong, and P. Schlottmann, Solid State Commun. **148**, 305 (2008).
[13] M. Schneider, D. Geiger, S. Esser, U. S. Pracht, C. Stingl, Y. Tokiwa, V. Moshnyaga, I. Sheikin, J. Mravlje, M. Scheffler, and P. Gegenwart, Phys. Rev. Lett. **112**, 206403 (2014).
[14] S. Middey, P. Mahadevan, and D. D. Sarma, Phys. Rev. B **83**, 014416 (2011).
[15] E. Jakobi, S. Kanungo, S. Sarkar, S. Schmitt, and T. Saha-Dasgupta, Phys. Rev. B **83**, 041103(R) (2011).
[16] L. de' Medici, J. Mravlje, and A. Georges, Phys. Rev. Lett. **107**, 256401 (2011).
[17] I. I. Mazin and D. J. Singh, Phys. Rev. B **56**, 2556 (1997).
[18] J. M. Rondinelli, N. M. Caffrey, S. Sanvito, and N. A. Spaldin, Phys. Rev. B **78**, 155107 (2008).
[19] H. Hadipour and M. Akhavan, Eur. Phys. J. B **84**, 203 (2011).
[20] G. T. Wang, M. P. Zhang, Z. X. Yang, and Z. Fang, J. Phys.: Condens. Matter **21**, 265602 (2009).
[21] M. Kim and B. I. Min, Phys. Rev. B **91**, 205116 (2015).
[22] R. S. Singh, V. R. R. Medicherla, and K. Maiti, Physica B **403**, 1398 (2008).
[23] K. Maiti and R. S. Singh, Phys. Rev. B **71**, 161102(R) (2005).
[24] J. Kim, J.-Y. Kim, B.-G. Park, and S.-J. Oh, Phys. Rev. B **73**, 235109 (2006).
[25] W. Siemons, G. Koster, A. Vailionis, H. Yamamoto, D. H. A. Blank, and M. R. Beasley, Phys. Rev. B **76**, 075126 (2007).
[26] J. Okamoto, T. Mizokawa, A. Fujimori, I. Hase, M. Nohara, H. Takagi, Y. Takeda, and M. Takano, Phys. Rev. B **60**, 2281 (1999).
[27] J. Park, S. J. Oh, J. H. Park, D. M. Kim, and C. B. Eom, Phys. Rev. B **69**, 085108 (2004).
[28] S. Grebinskij, S. Masys, S. Mickevicius, V. Lisauskas, and V. Jonauskas, Phys. Rev. B **87**, 035106 (2013).
[29] K. Maiti, R. S. Singh, and V. R. R. Medicherla, Europhys. Lett. **78**, 17002 (2007).
[30] D. W. Jeong, H. C. Choi, C. H. Kim, S. H. Chang, C. H. Sohn, H. J. Park, T. D. Kang, D.-Y. Cho, S. H. Baek, C. B. Eom, J. H. Shim, J. Yu, K. W. Kim, S. J. Moon, and T. W. Noh, Phys. Rev. Lett. **110**, 247202 (2013).
[31] C.-Q. Jin, J.-S. Zhou, J. B. Goodenough, Q. Q. Liu, J. G. Zhao, L. X. Yang, Y. Yu, R. C. Yu, T. Katsura, A. Shatskiy, and E. Ito, Proc. Natl. Acad. Sci. USA **105**, 7115 (2008).
[32] A. Georges, Luca de' Medici, and J. Mravlje, Annu. Rev. Condens. Matter Phys. **4**, 137 (2013).
[33] H. T. Dang, J. Mravlje, A. Georges, and A. J. Millis, Phys. Rev. B **91**, 195149 (2015).
[34] B. J. Kim, H. Jin, S. J. Moon, J.-Y. Kim, B.-G. Park, C. S. Leem, J. Yu, T. W. Noh, C. Kim, S.-J. Oh, J.-H. Park, V. Durairaj, G. Cao, and E. Rotenberg, Phys. Rev. Lett. **101**, 076402 (2008).
[35] H. F. Yang, Z. T. Liu, C. C. Fan, Q. Yao, P. Xiang, K. L. Zhang, M. Y. Li, H. Li, J. S. Liu, D. W. Shen, and M. H. Jiang, Phys. Rev. B **93**, 121102(R) (2016).
[36] M. Y. Li, Z. T. Liu, H. F. Yang, J. L. Zhao, Q. Yao, C. C. Fan, J. S. Liu, B. Gao, D. W. Shen, and X. M. Xie, Chin. Phys. Lett. **32**, 057402 (2015).
[37] D. L. Proffit, H. W. Jang, S. Lee, C. T. Nelson, X. Q. Pan, M. S. Rzchowski, and C. B. Eom, Appl. Phys. Lett. **93**, 111912 (2008).
[38] C. Y. Chen, J. Avila, E. Frantzeskakis, A. Levy, and M. C. Asensio, Nat. Commun. **6**, 8585 (2015).
[39] S.-K. Mo, J. D. Denlinger, H.-D. Kim, J.-H. Park, J. W. Allen, A. Sekiyama, A. Yamasaki, K. Kadono, S. Suga, Y. Saitoh, T. Muro, P. Metcalf, G. Keller, K. Held, V. Eyert, V. I. Anisimov, and D. Vollhardt, Phys. Rev. Lett. **90**, 186403 (2003).
[40] H. C. Xu, Y. Zhang, M. Xu, R. Peng, X. P. Shen, V. N. Strocov, M. Shi, M. Kobayashi, T. Schmitt, B. P. Xie, and D. L. Feng, Phys. Rev. Lett. **112**, 087603 (2014).
[41] A. Georges, G. Kotliar, W. Krauth, and M. J. Rozenberg, Rev. Mod. Phys. **68**, 13 (1996).

[42] G. Kotliar and D. Vollhardt, Phys. Today **57**, 53 (2004).
[43] E. Gorelov, M. Karolak, T. O. Wehling, F. Lechermann, A. I. Lichtenstein, and E. Pavarini, Phys. Rev. Lett. **104**, 226401 (2010).
[44] M. Neupane, P. Richard, Z.-H. Pan, Y. M. Xu, R. Jin, D. Mandrus, X. Dai, Z. Fang, Z. Wang, and H. Ding, Phys. Rev. Lett. **103**, 097001 (2009).
[45] K. Haule and G. Kotliar, New J. Phys. **11**, 025021 (2009).
[46] Z. P. Yin, K. Haule, and G. Kotliar, Nat. Mater. **10**, 932 (2011).
[47] D. J. Singh, J. Appl. Phys. **79**, 4818 (1996).
[48] S. Tripathi, R. Rana, S. Kumar, P. Pandey, R. S. Singh, and D. S. Rana, Sci. Rep. **4**, 3877 (2014).
[49] A. T. Zayak, X. Huang, J. B. Neaton, and K. M. Rabe, Phys. Rev. B **77**, 214410 (2008).
[50] G. Cao, S. McCall, M. Shepard, J. E. Crow, and R. P. Guertin, Phys. Rev. B **56**, 321 (1997).
[51] Z. Fang, N. Nagaosa, K. S. Takahashi, A. Asamitsu, R. Mathieu, T. Ogasawara, H. Yamada, M. Kawasaki, Y. Tokura, and K. Terakura, Science **302**, 92 (2003).
[52] K. Yoshimura, T. Imai, T. Kiyama, K. R. Thurber, A. W. Hunt, and K. Kosuge, Phys. Rev. Lett. **83**, 4397 (1999).